Supporting Information for

CPO2Hill: An Efficient Parametrization to Infer Anisotropic Viscous Behaviour Directly from Olivine Texture Parameters

Á. Király[1,2*], Y. Wang[2,3], C.P. Conrad[2], L.N. Hansen[4], B. Mather[5]

[1] NJORD Centre, University of Oslo, Oslo, Norway

[2] Centre for Planetary Habitability, University of Oslo, Oslo, Norway

[3] GFZ Helmholtz Centre for Geosciences, Potsdam, Germany

[4] Department of Earth and Environmental Sciences, University of Minnesota, Minneapolis, MN, USA

[5] EarthByte Group, School of Geosciences, University of Sydney, Sydney, NSW, Australia

[*]Corresponding author: Ágnes Király (agnes.kiraly@geo.uio.no)

Contents of this file

Introduction

Here, we provide additional information related to the methodology of approximating the CPO reference frame (Text S1), and additional figures related to the methodology (Figure S1, S2, S3) and results (Figures S4-S20).

Text S1 – CPO Reference Frame

We approximate the distribution of grain orientations with a second order orientation tensor, which can be calculated as the covariance matrix of all individual grain orientations. We do this for all three symmetry axes of olivine. To define the mean orientation of the CPO, we calculate the eigenvectors of the three covariance matrices. The eigenvectors with the highest eigenvalues represent the mean (second order) orientation of the olivine [100]-, [010]-, and [001]-axes. In cases where the CPO is more complex than can be fully described using a second order tensor (i.e. by degree 2 harmonics), the three eigenvectors defining the mean orientations of the individual axes might not form an orthogonal basis. In other cases, for example a fully girdle pattern on the [010] and [001] axes, there are just simply no one best solutions for the reference frame, and it is possible that the eigen vectors for the two axes point in the same direction.

There are several strategies to correct for this. In the database, we fix the mean orientation of the [100]-axis to the direction of its eigenvector and re-orient the mean [010]- and [001]-axes around this mean [100]-axis orientation. This choice was made as previous studies often relate the anisotropy to the mean [100] direction. To apply this method, we project the eigenvector of the mean [010]-axis onto the [100]-axis and correct the eigenvector using the projection. After this, the corrected mean [010]-axis orientation should not make a shadow on the [100]-axis, that is, their vector products equate to 0. Once we corrected the mean [010]-axis orientation, the mean [001]-axis results from the cross product of the mean [100]-axis and the mean [010]-axis.

Another option for enforcing orthogonality is to use singular value decomposition (SVD), which yields an orthonormal set of unit vectors spanning the same subspace as the eigenvectors of the second-order orientation tensor. A further possibility, although less practical when the CPO is represented by a discrete set of Euler angles, is to determine the maximum of the orientation density function (max(ODF)). This can be computed using MTEX (Mainprice et al., 2015). Both the SVD and the max(ODF) method might result in a mean [100] direction that is different from the eigen vector of the second order orientation tensor, as they can be impacted by the distribution of the other two axes.

Supplementary Figures

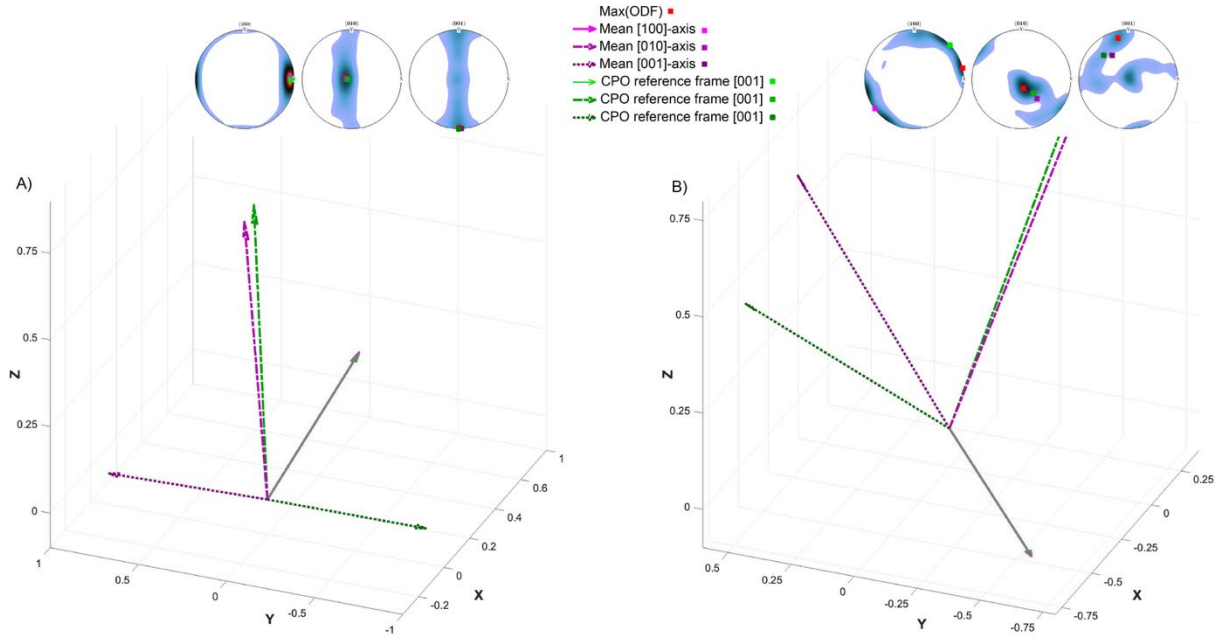

Figure S1. Mean CPO definition for a simple ("Bingham") texture, and for a complex texture with multiple maxima. Magenta arrows show the unit eigenvectors of the mean [100]- (solid line), [010]- (dashed line) and [001]- (dotted line) axes orientations, while the green arrows represent the corrected, orthogonal, CPO reference frame. These orientations are also shown as colored squares on the stereograph plots of the ODF, together with the result of the max(ODF) MTEX function (red squares).

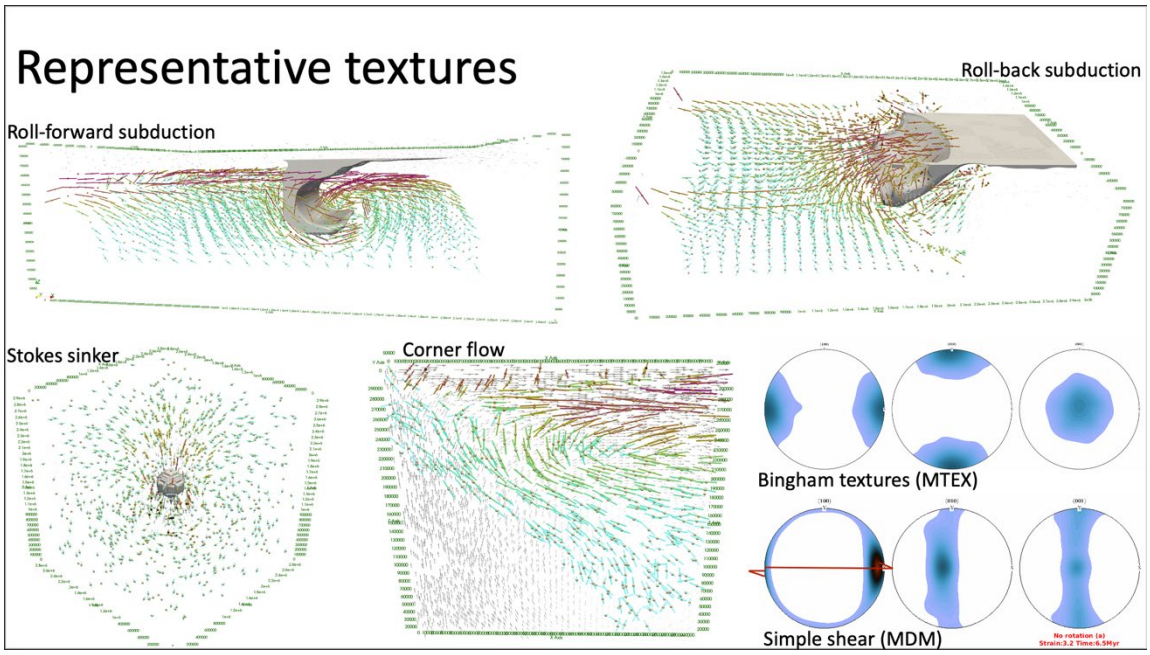

Figure S2. The database built from representative textures from geodynamic models run in ASPECT, here shown as snapshots that depict the mean [100] symmetry axis orientation. Additional textures are added to the database from a simple shear model (Király et al., 2020) and further "Bingham textures" directly generated with MTEX (Mainprice et al., 2015).

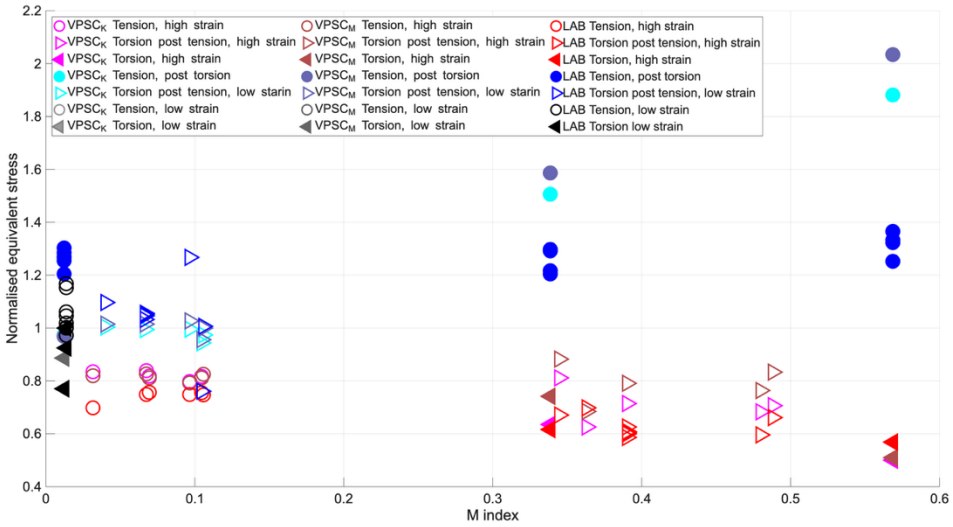

Figure S3. Comparison of VPSC simulations against laboratory data (Hansen et al., 2012, 2016) following (Mameri et al., 2019). $VPSC_K$ symbols (this study) show results from VPSC simulations using the CRSS for olivine slip systems listed in the main text Table 1. $VPSC_M$ symbols show results from VPSC simulations using the parameters from Mameri et al., 2019. Laboratory equivalent stresses have been rescaled to a fix equivalent strain rate following (Mameri et al., 2019), and each data point is normalized by the calculated or measured equivalent stress of an isotropic aggregate.

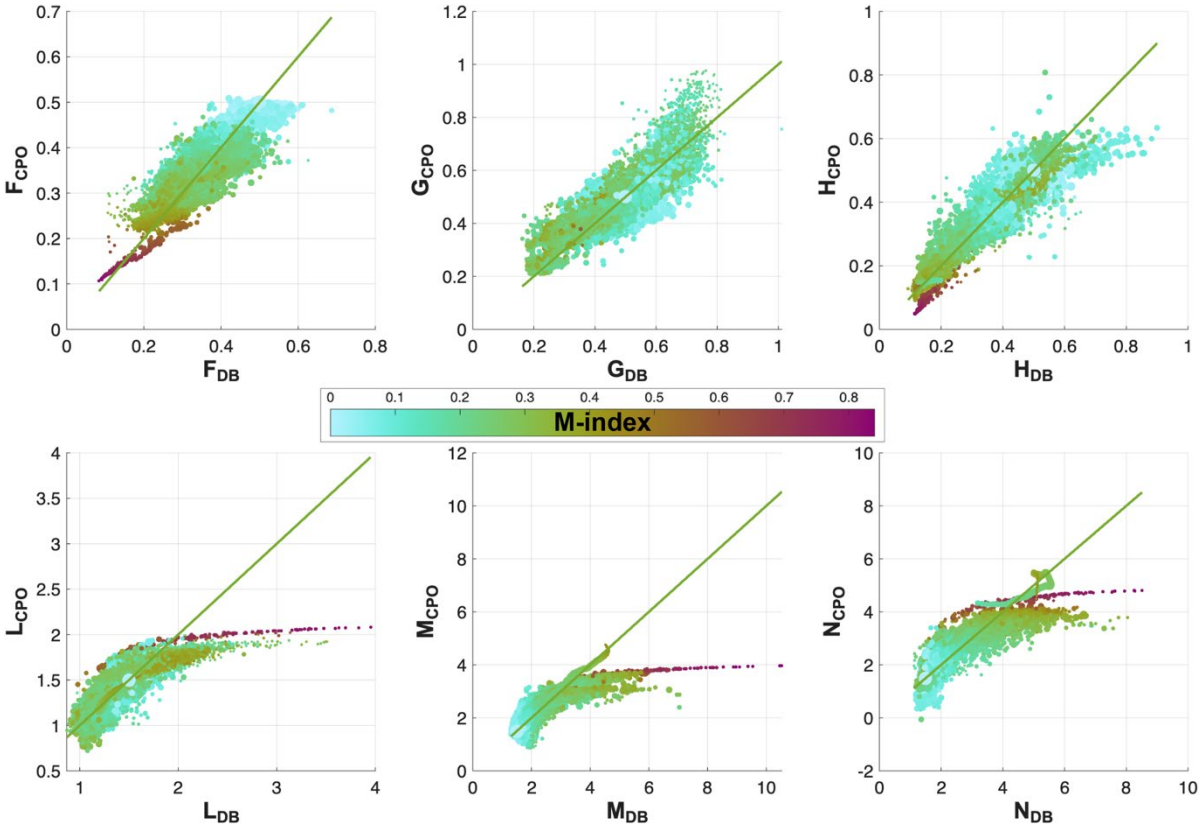

Figure S4. Linear regression model results plotted against database entries for each Hill coefficient, computed using CPO2Hill model v1. All points are sized according to their weight in the linear regression model (*weight ~ 1/error*) and colored according to the M-index of the corresponding texture.

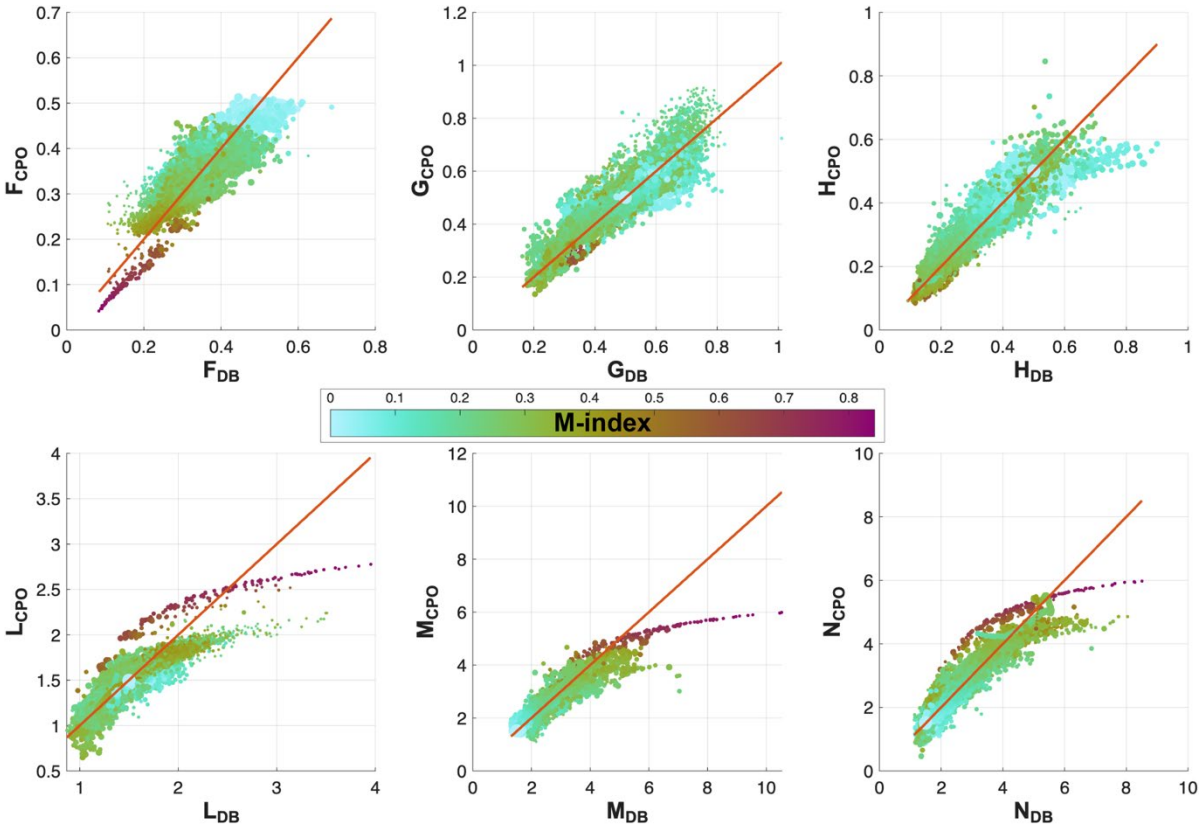

Figure S5. Linear regression model results plotted against database entries for each Hill coefficient, computed using CPO2Hill model v2. All points are sized according to their weight in the linear regression model (*weight ~ 1/error*) and colored according to the M-index of the corresponding texture.

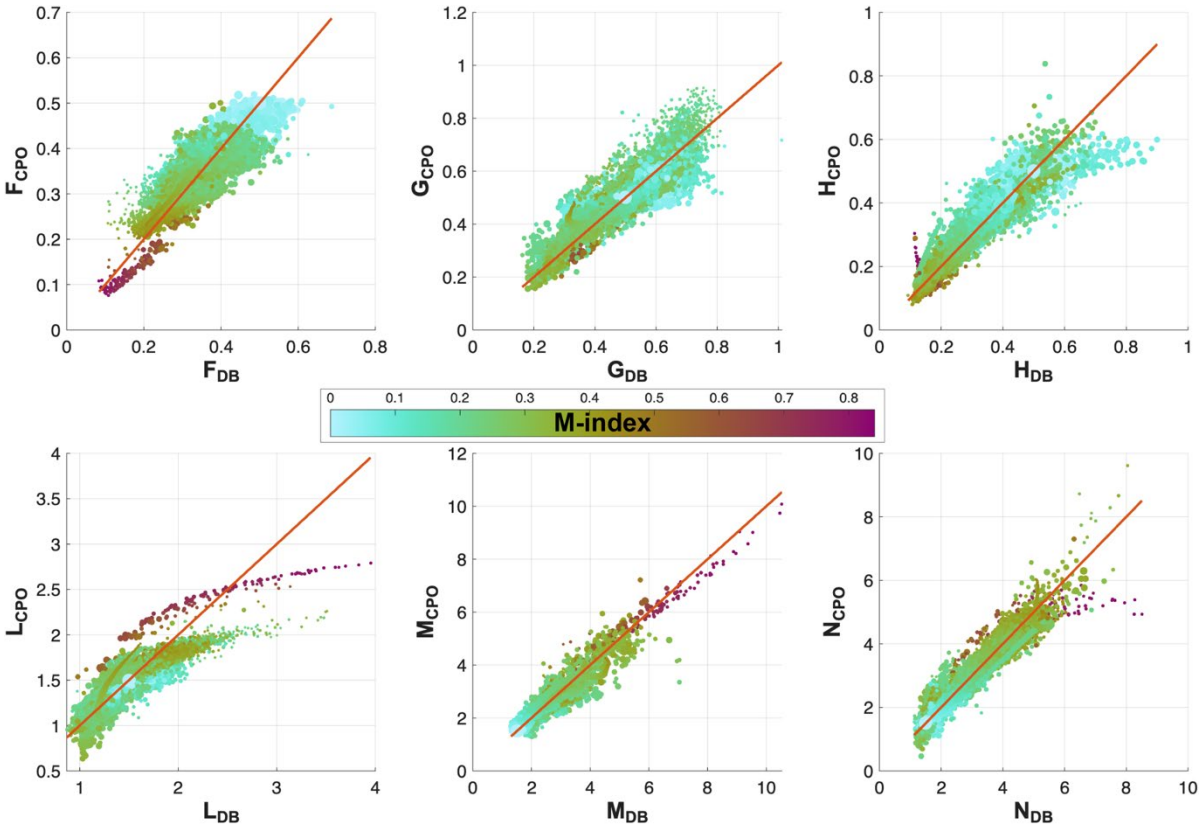

Figure S6. Linear regression model results plotted against database entries for each Hill coefficient, computed using CPO2Hill model v3. All points are sized according to their weight in the linear regression model (*weight ~ 1/error*) and colored according to the M-index of the corresponding texture.

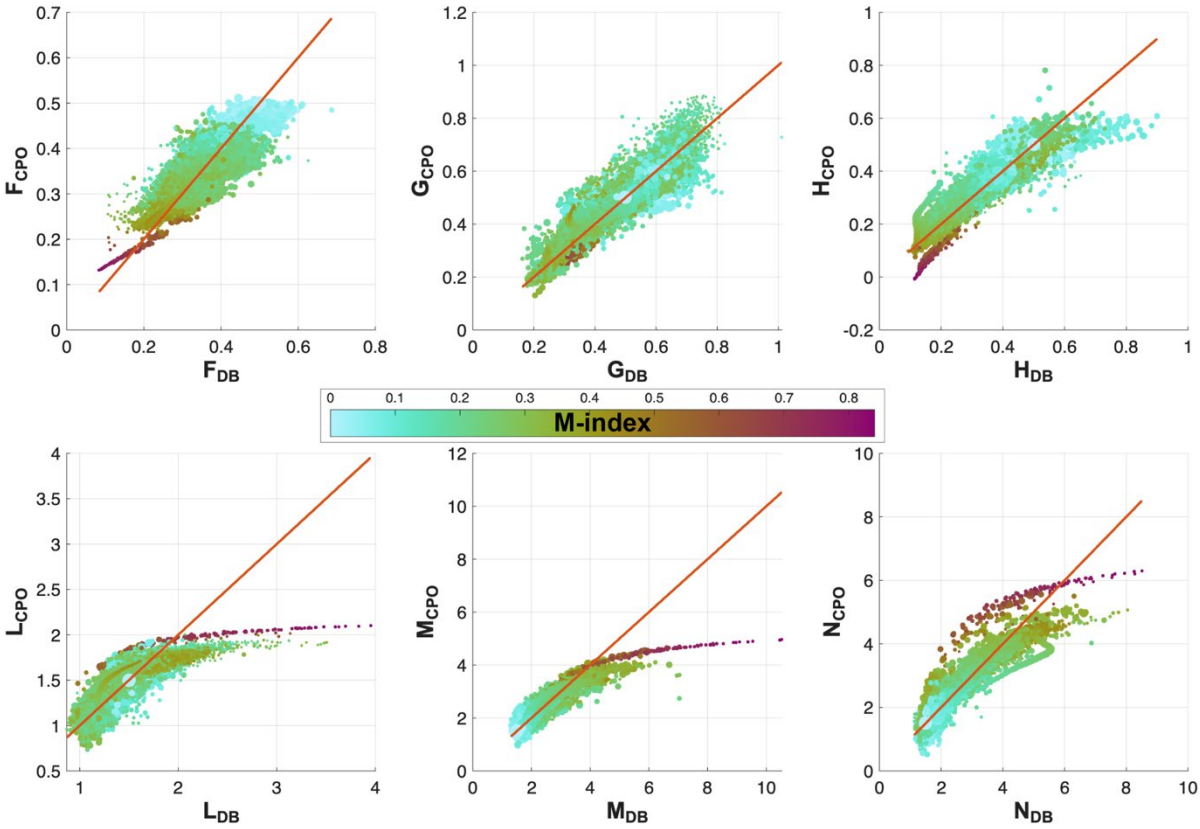

Figure S7. Linear regression model results plotted against database entries for each Hill coefficient, computed using CPO2Hill model v4. All points are sized according to their weight in the linear regression model (*weight ~ 1/error*) and colored according to the M-index of the corresponding texture.

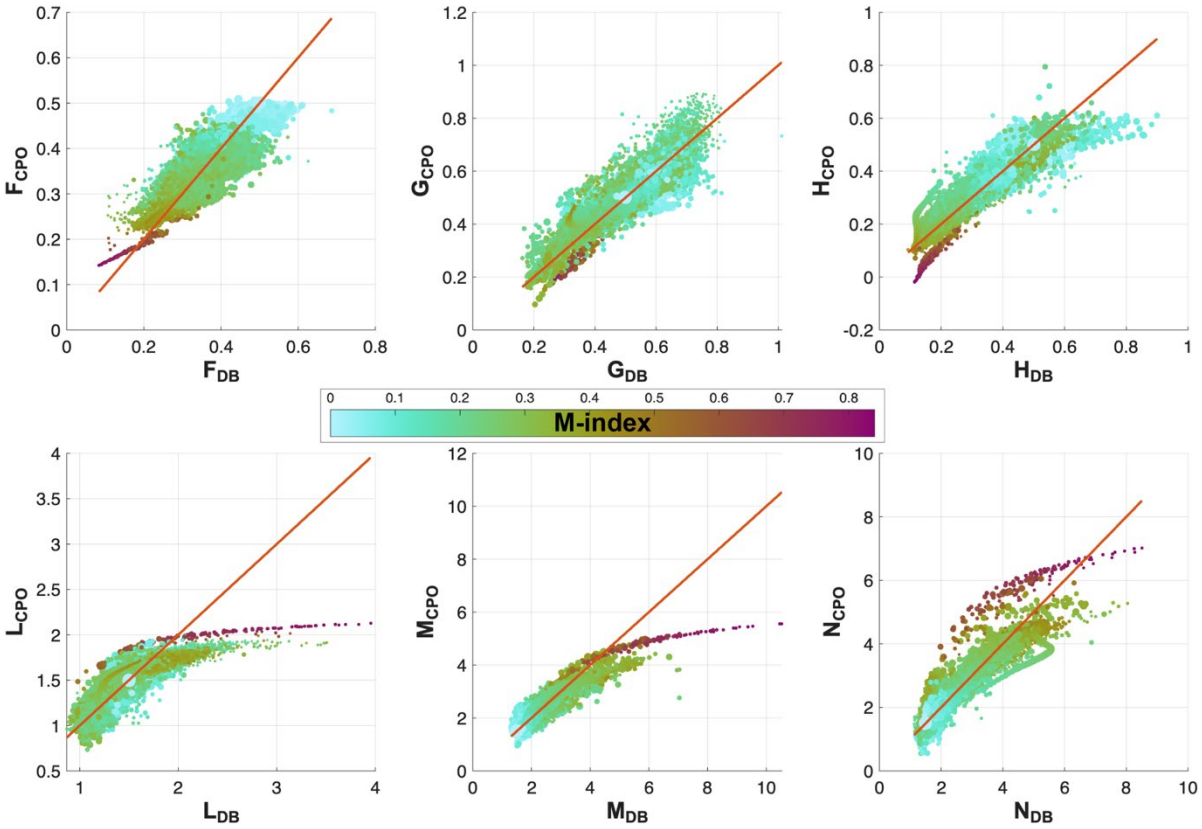

Figure S8. Linear regression model results plotted against database entries for each Hill coefficient, computed using CPO2Hill model v5. All points are sized according to their weight in the linear regression model (*weight ~ 1/error*) and colored according to the M-index of the corresponding texture.

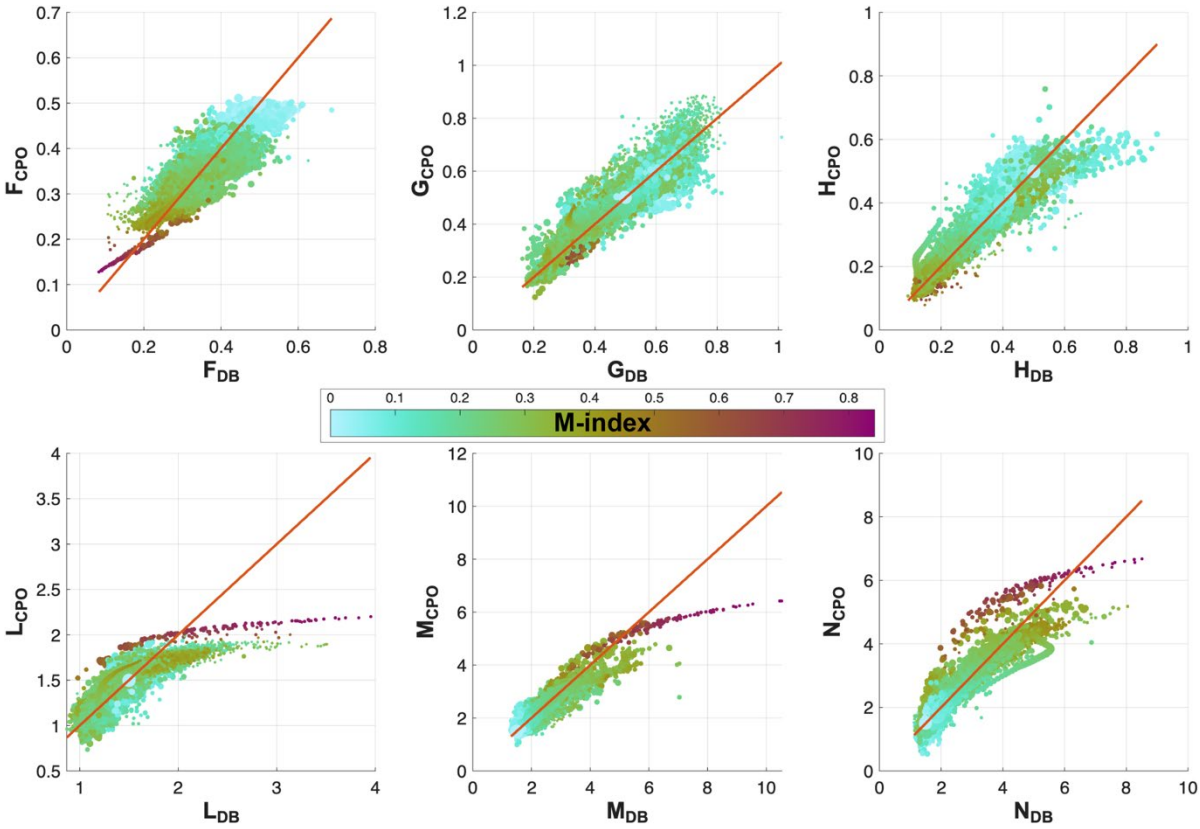

Figure S9. Linear regression model results plotted against database entries for each Hill coefficient, computed using CPO2Hill model v6. All points are sized according to their weight in the linear regression model (*weight ~ 1/error*) and colored according to the M-index of the corresponding texture.

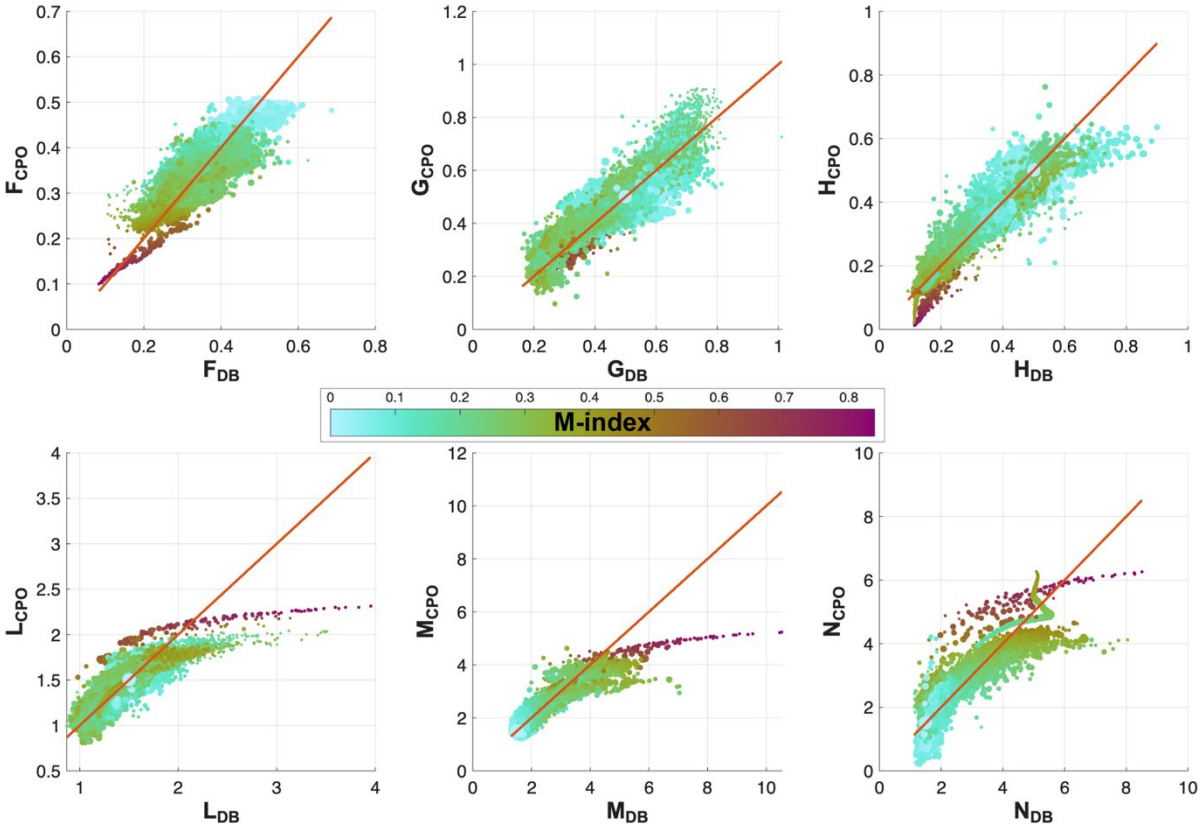

Figure S10. Linear regression model results plotted against database entries for each Hill coefficient, computed using CPO2Hill model v7. All points are sized according to their weight in the linear regression model (*weight ~ 1/error*) and colored according to the M-index of the corresponding texture.

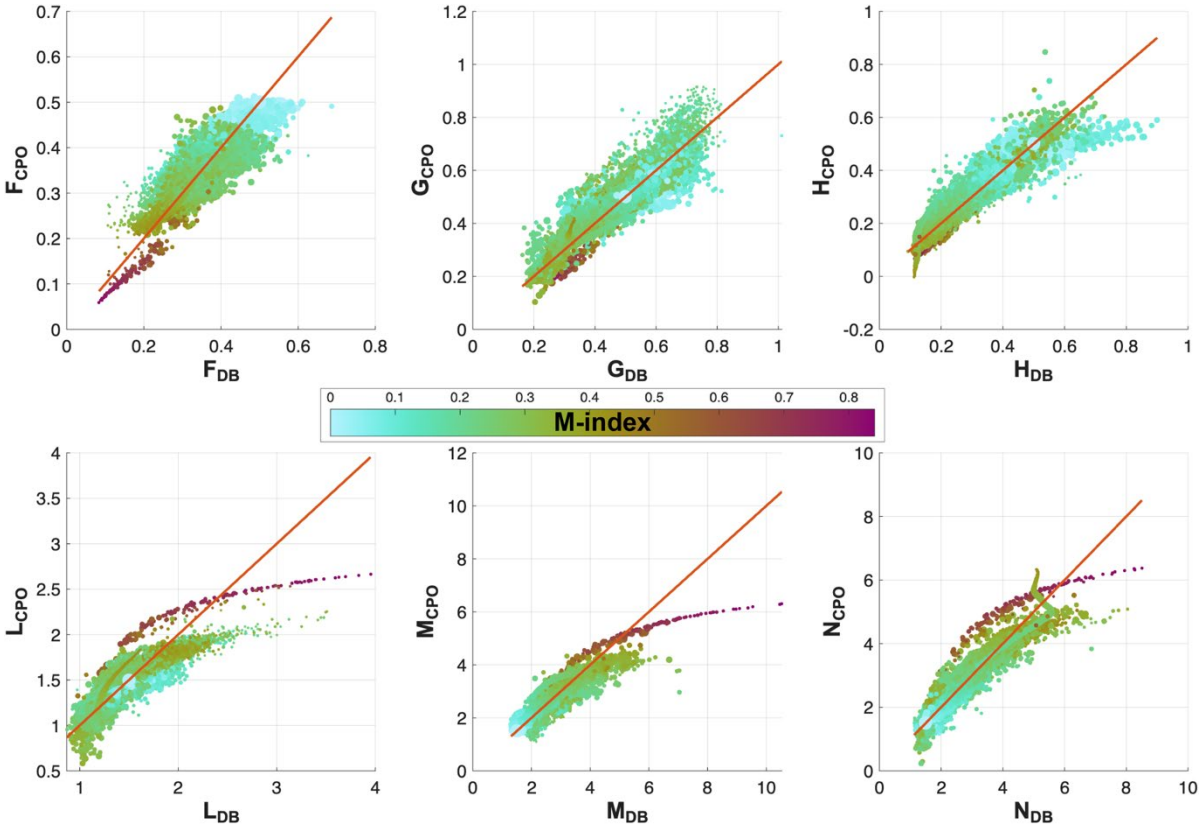

Figure S11. Linear regression model results plotted against database entries for each Hill coefficient, computed using CPO2Hill model v8. All points are sized according to their weight in the linear regression model (*weight ~ 1/error*) and colored according to the M-index of the corresponding texture.

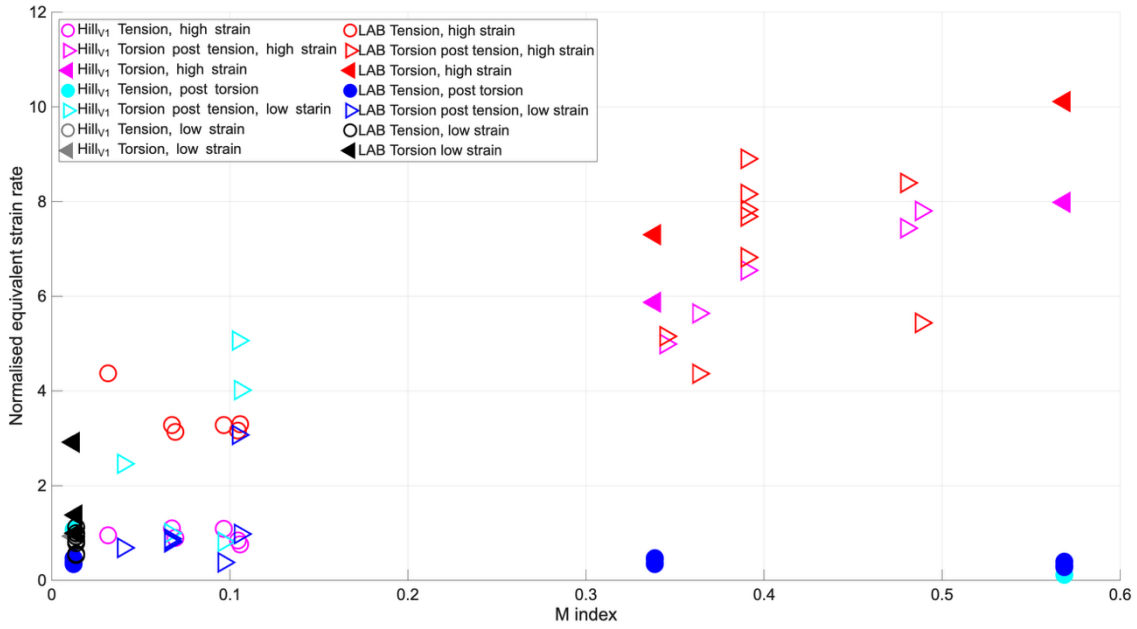

Figure S12. Laboratory experimental data (Hansen et al., 2012, 2016) compared to CPO2Hill model v1 predictions.

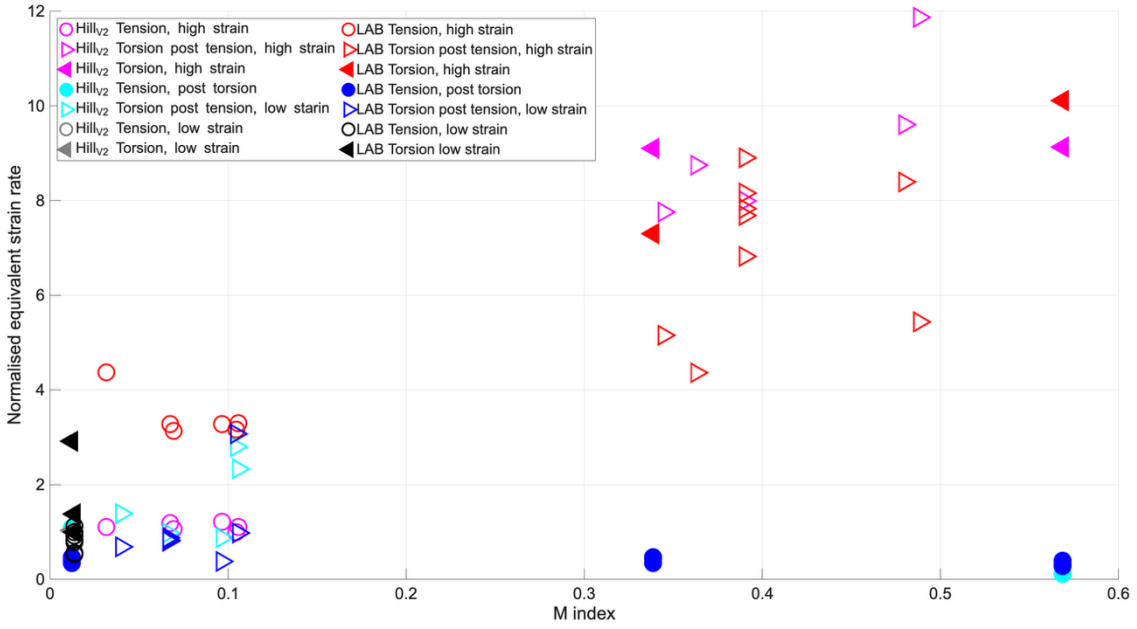

Figure S13. Laboratory experimental data (Hansen et al., 2012, 2016) compared to CPO2Hill model v2 predictions.

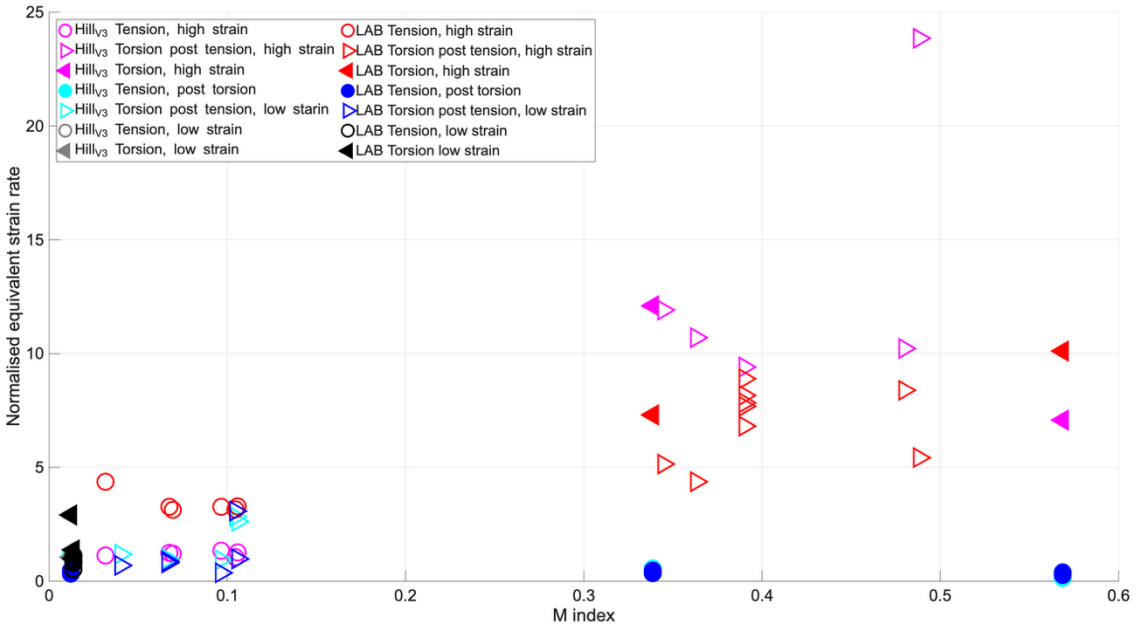

Figure S14. Laboratory experimental data (Hansen et al., 2012, 2016) compared to CPO2Hill model v3 predictions.

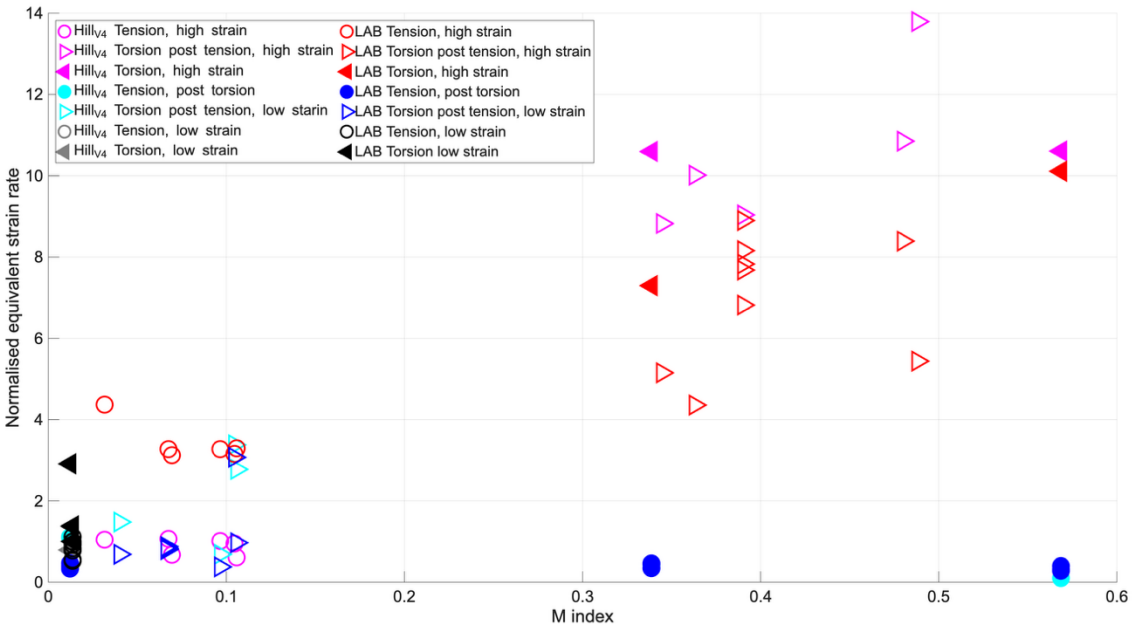

Figure S15. Laboratory experimental data (Hansen et al., 2012, 2016) compared to CPO2Hill model v4 predictions.

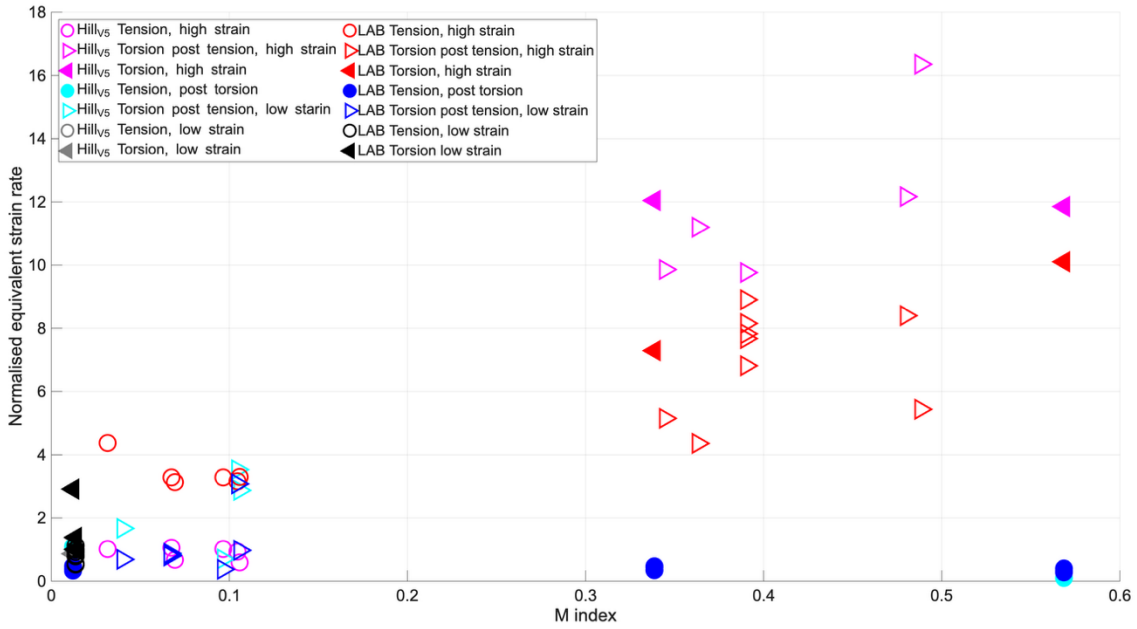

Figure S16. Laboratory experimental data (Hansen et al., 2012, 2016) compared to CPO2Hill model v5 predictions.

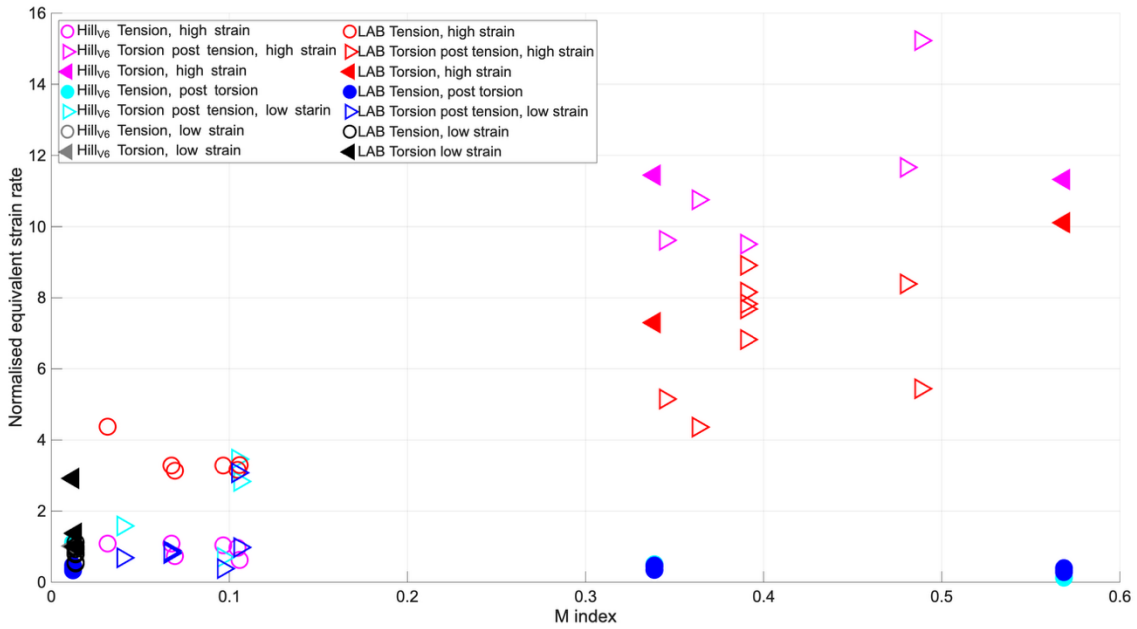

Figure S17. Laboratory experimental data (Hansen et al., 2012, 2016) compared to CPO2Hill model v6 predictions.

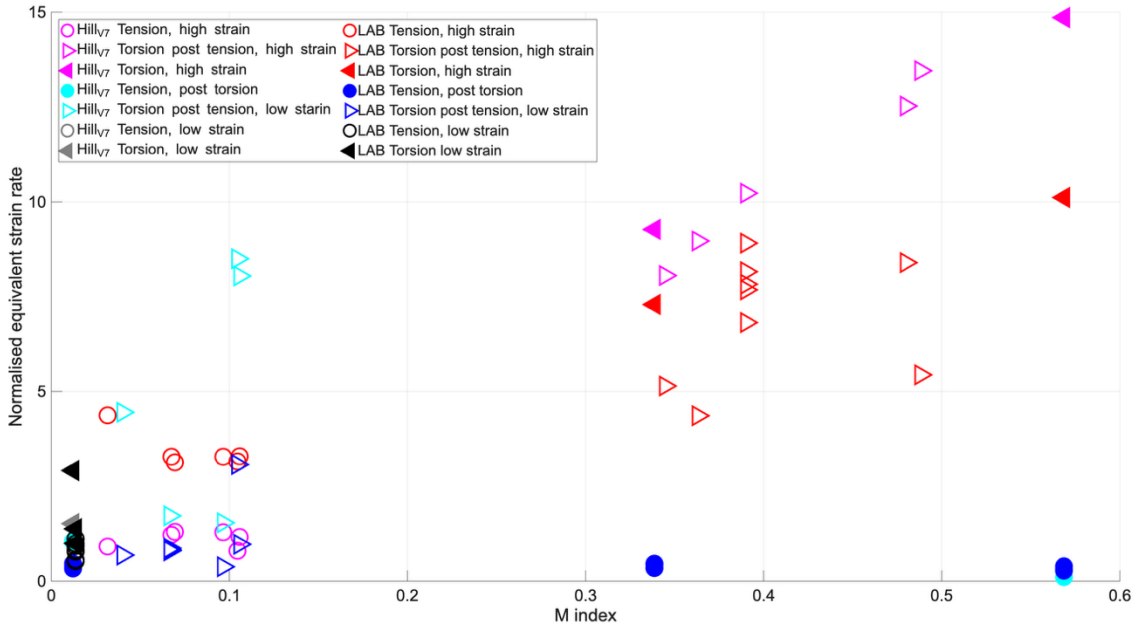

Figure S18. Laboratory experimental data (Hansen et al., 2012, 2016) compared to CPO2Hill model v7 predictions.

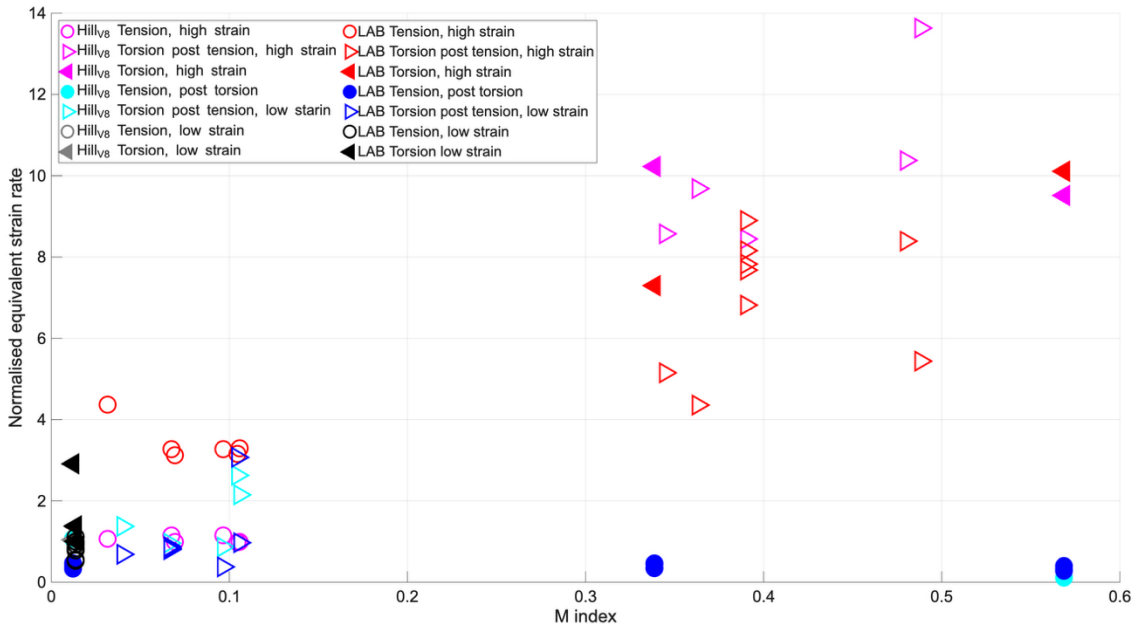

Figure S19. Laboratory experimental data (Hansen et al., 2012, 2016) compared to CPO2Hill model v8 predictions.

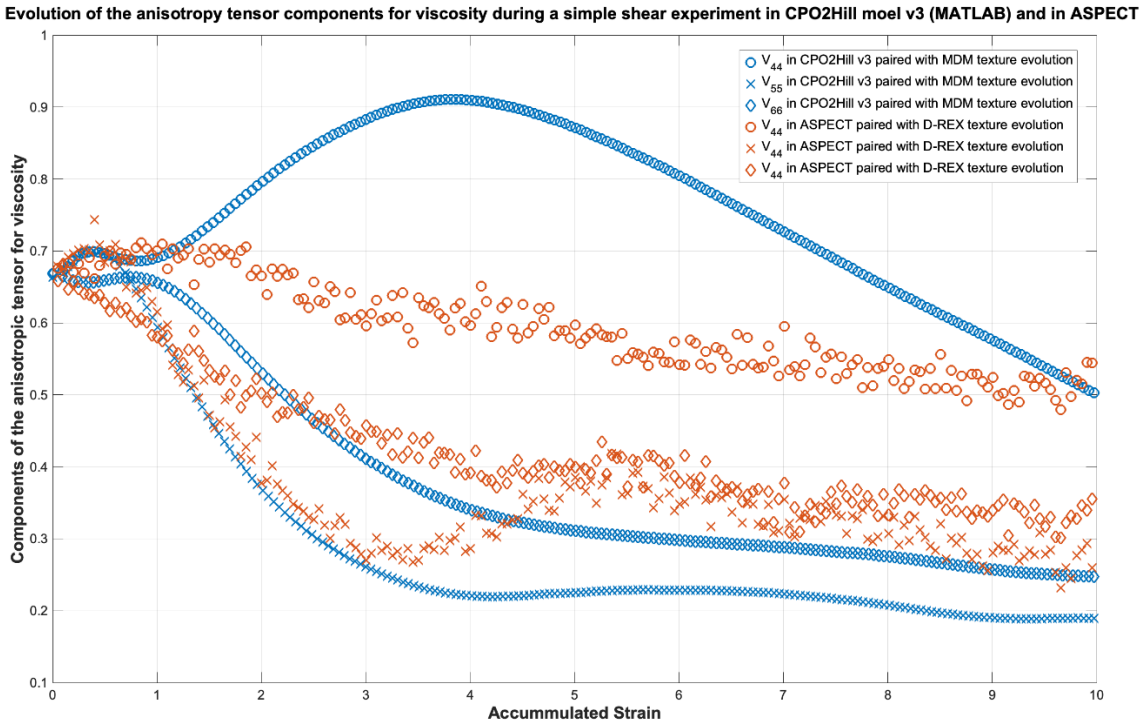

Figure S20. Results from simple shear model run in ASPECT compared to modeling results obtained in MATLAB using the CPO2Hill v3 model. Here we plot the components of the anisotropic tensor for viscosity (V_{44}, V_{55}, and V_{66} in Kelvin notation) which are the most important components relating shear stresses (σ_{23}, σ_{13} and σ_{12}, respectively) to shear strain rates ($\dot{\varepsilon}_{23}, \dot{\varepsilon}_{13}$, and $\dot{\varepsilon}_{12}$).